

THE ORBITAL STATISTICS OF STELLAR INSPIRAL AND RELAXATION NEAR A MASSIVE BLACK HOLE: CHARACTERIZING GRAVITATIONAL WAVE SOURCES

CLOVIS HOPMAN¹ AND TAL ALEXANDER^{1,2}

Draft version May 23, 2019

ABSTRACT

We study the orbital parameters distribution of stars that are scattered into nearly radial orbits and then spiral into a massive black hole (MBH) due to dissipation, in particular by emission of gravitational waves (GW). This is important for GW detection, e.g. by the *Laser Interferometer Space Antenna (LISA)*. Signal identification requires knowledge of the waveforms, which depend on the orbital parameters. We use analytical and Monte Carlo methods to analyze the interplay between GW dissipation and scattering in the presence of a mass sink during the transition from the initial scattering-dominated phase to the final dissipation-dominated phase of the inspiral. Our main results are (1) Stars typically enter the GW-emitting phase with high eccentricities. (2) The GW event rate per galaxy is $\text{few} \times 10^{-9} \text{ yr}^{-1}$ for typical central stellar cusps, almost independently of the relaxation time or the MBH mass. (3) For intermediate mass black holes (IBHs) of $\sim 10^3 M_{\odot}$ such as may exist in dense stellar clusters, the orbits are very eccentric and the inspiral is rapid, so the sources are very short-lived.

Subject headings: black hole physics — stellar dynamics — gravitational waves

1. INTRODUCTION

Dissipative interactions between stars and massive black holes (MBHs; $M_{\bullet} \gtrsim 10^6 M_{\odot}$) in galactic nuclei (e.g. Gebhardt et al. 2000, 2003), or intermediate mass black holes (IBHs; $10^2 < M_{\bullet} \lesssim 10^4 M_{\odot}$), which may exist in dense stellar clusters, have been in the focus of several recent studies. The interest is mainly motivated by the possibility of using the dissipated power to detect the BH, or to probe General Relativity. Examples of such processes are tidal heating (e.g. Alexander & Morris 2003; Hopman, Portegies Zwart & Alexander 2004) and gravitational wave (GW) radiation (Hils & Bender 1995; Sigurdsson & Rees 1997; Ivanov 2002; Freitag 2001, 2003).

A statistical characterization of inspiral orbits is of interest in anticipation of GW observations by the Laser Interferometer Space Antenna (*LISA*). *LISA* will be able to observe GW from stars at cosmological distances during the final, highly relativistic phase of inspiral into a $\sim 10^6 M_{\odot}$ MBH, thereby opening a new non-electromagnetic astronomical window. GW from inspiraling compact objects (COs) is one of the three major targets of the *LISA* mission (Barack & Cutler 2003, 2004; Gair et al. 2004), together with cosmological MBH–MBH mergers and Galactic CO–CO mergers.

LISA can detect GW emission from stars with orbital period shorter than $P_L \sim 10^4$ s. In order for the shortest possible period to be small enough to be detectable by *LISA*, the MBH has to be of moderate mass, $M_{\bullet} \lesssim 5 \times 10^6 M_{\odot}$ (Sigurdsson & Rees 1997). *LISA* is expected to be able to detect inspiral into MBHs of $10^6 M_{\odot}$ to distances as far as $\gtrsim 1$ Gpc.

The detailed time-evolution of the GW depends on the eccentricity of the stellar orbit, and therefore probes both General Relativity and the statistical predictions of stellar dynamics theory. Due to the low signal to noise ratio, knowledge of the wave forms is required in advance. For this purpose, it is necessary to estimate the orbital characteristics of the

GW-emitting stars, and in particular the distribution function (DF) of their eccentricities (Pierro et al. 2001; Glampedakis, Hughes & Kennefick 2002), as the wave forms are strong functions of the eccentricity (e.g. Barack & Cutler 2003; Wen & Gair 2005). This study focuses on inspiral by GW emission. However, it should be emphasized that inspiral is a general consequence of dissipation, and the formalism presented below can be extended in a straight-forward way to other dissipation processes, such as tidal heating.

The *prompt infall* of a star into a MBH and its destruction have been studied extensively (§2.1). Here we analyze a different process, the *slow inspiral* of stars (Alexander & Hopman 2003). A star on a highly eccentric orbit with small periastron r_p , repeatedly loses some energy ΔE every periastron passage due to GW emission, and its orbit gradually decays. At a distance r_0 from the MBH, where the orbital period is P_0 , the time-scale t_0 for completing the inspiral (i.e. decaying to a $P \rightarrow 0$ orbit) is much longer than the time-scale P_0 needed to reach the MBH directly on a nearly radial orbit. While the orbit decays, two-body scatterings by other stars continually perturb it, changing its orbital angular momentum J by order unity on a timescale t_J . Because $t_0 \gg P_0$, inspiraling stars are much more susceptible to scattering than those on infall orbits. If $t_0 > t_J$, either because r_0 is large or r_p is large (small ΔE), then the orbit will not have time to decay and reach an observationally interesting short period. Before that can happen, the star will either be scattered to a wider orbit where energy dissipation is no longer efficient, or conversely, plunge into the MBH. Inspiral is thus much rarer than direct infall. The stellar consumption rate, and hence the properties of the stellar distribution function (DF) at low J , are dominated by prompt infall, with inspiral contributing only a small correction. This DF describes the parent population of the inspiraling stars.

We show below that the DF of the small subset of stars on low- J orbits that complete the inspiral and are GW sources is very different from that of the parent population (Fig. 2). This results from the interplay between GW dissipation and scattering in the presence of a mass sink during the transition ($t_0 \sim t_J$) from the initial scattering-dominated phase to the

¹ Center for Astrophysics, Faculty of Physics, Weizmann Institute of Science, POB 26, Rehovot 76100, Israel; clovis.hopman@weizmann.ac.il, tal.alexander@weizmann.ac.il

² Incumbent of the William Z. & Eda Bess Novick career development chair

final dissipation-dominated phase of the inspiral.

This paper is organized as follows. In §2 we recapitulate some of the results of loss cone theory for the prompt infall, and extend it to slow inspiral. In §3 and §4 we present a detailed analytical discussion of the main effects that determine the rates of GW events and their statistical properties. In §4 we describe three different approaches for studying the problem: by Monte Carlo simulations, by solving numerically the 2D diffusion / dissipation equation in E and J , and by a simplified analytical model, which mimics the behavior of a typical star. In §5 we apply the MC simulation to a MBH in a galactic nucleus, and an IBH in a stellar cluster. We summarize our results in §6.

2. THE LOSS-CONE

The rate at which stars are consumed by an MBH and the effect this has on the stellar DF near it have been studied extensively (Peebles 1972; Frank & Rees 1976; Bahcall & Wolf 1976, 1977; Lightman and Shapiro 1977; Cohn & Kulsrud 1978; Syer & Ulmer 1999; Magorrian & Tremaine 1999; Miralda-Escudé & Gould 2000; Freitag & Benz 2001; Alexander & Hopman 2003; Wang & Merritt 2004; see Sigurdsson 2003 for a comparative review). Self-consistent N-body simulations with stellar captures were recently performed by Baumgardt, Makino, & Ebisuzaki (2004a, 2004b) and by Preto, Merritt & Spurzem (2004).

We begin by summarizing these results, neglecting dissipative processes. We then extend the formalism to include dissipative processes.

2.1. Prompt infall

The stellar orbits are defined by a specific angular momentum J and relative specific energy $\varepsilon = \psi(r) - v^2/2$ (hereafter “angular momentum” and “energy”), where ψ is the relative gravitational potential, and v is the velocity of a star with respect to the MBH. A spherical mass distribution and a nearly spherical velocity distribution are assumed.

Orbits in the Schwarzschild metric (unlike Keplerian orbits) can escape the MBH only if their angular momentum is high enough, $J > J_{lc}(\varepsilon)$. The phase space volume $J < J_{lc}$ is known as the “loss-cone”. As argued below, stars that are scattered to low- J orbits are typically on nearly zero-energy orbits. For such orbits

$$J_{lc}(\varepsilon=0) = \frac{4GM_{\bullet}}{c}, \quad (1)$$

The size of the loss-cone J_{lc} is nearly constant over the relevant range of ε . Only during the very last in-spiral phase the energy of the star becomes non-negligible compared to its rest-mass, in which case the loss-cone is slightly modified (see section [4.1]). Deviations from geodesic motion due to tidal interactions are neglected here. This assumption is justified for COs orbiting $\sim 10^6 M_{\odot}$ MBHs, where the tidal radius is much smaller than the event horizon. For main-sequence (MS) stars where the tidal radius lies outside the event horizon, the loss-cone is similarly defined as the minimal J required to avoid tidal disruption.

Stars that are initially on orbits with $J < J_{lc}$ will promptly fall into the MBH on an orbital timescale. Subsequently, the infall flow in J -space, $\mathcal{F}(\varepsilon; J)$, is set by the rate at which relaxation processes (here assumed to be multiple two-body scattering events) re-populate the loss-cone orbits.

Diffusion in ε -space occurs on the relaxation timescale,

$t_r \sim \varepsilon/\dot{\varepsilon}$, whereas diffusion in J -space occurs on the angular momentum relaxation timescale,

$$t_J \sim J^2/(\dot{J}^2) \sim [J/J_m(\varepsilon)]^2 t_r, \quad (2)$$

where $J_m(\varepsilon)$ is the maximal (circular orbit) angular momentum for specific energy ε . The square root dependence of J on t_J reflects the random walk nature of the process. Typically, $J_{lc} \ll J_m$. In principle, stars can enter the loss-cone, $J < J_{lc}(\varepsilon)$ either by a decrease in J , or by an increase in ε (up to the last stable orbit). In practice, diffusion in J -space is much more efficient: the energy of a star must increase by many orders of magnitude in order for it to reach the loss-cone, which takes many relaxation times. The angular momentum of the star, on the other hand, needs only to change by order unity in order for the star to be captured, which happens on a much shorter time $t_J \leq t_r$.

The ratio between J_{lc} and the mean change in angular momentum per orbit, ΔJ , defines two dynamical regimes of loss-cone re-population (Lightman & Shapiro 1977). In the “Diffusive regime” of stars with large ε (tight orbits), $\Delta J \ll J_{lc}$ and so the stars slowly diffuse in J -space. The loss-cone remains nearly empty at all times since any star inside it is promptly swallowed. At $J \gg J_{lc}$ the DF is nearly isotropic, but it falls logarithmically to zero at $J \gtrsim J_{lc}$ (Eq. 10). In the “full loss-cone regime” (sometimes also called the “pin-hole” or “kick” regime) of stars with small ε (wide orbits), $\Delta J \gg J_{lc}$ and so the stars can enter and exit the loss-cone many times before reaching periaapse. As a result, the DF is nearly isotropic at all $J \gtrsim J_{lc}$. We argue below that only the diffusive regime is relevant for inspiral.

The DF in the diffusive regime is described by the Fokker-Planck equation. We follow Lightman & Shapiro (1977), who neglect the small contribution of energy diffusion to \mathcal{F} , and write the Fokker-Planck equation for the number density of stars $N(\varepsilon, J; t)$ as¹

$$\frac{\partial N(\varepsilon, J; t)}{\partial t} = -\frac{\partial \mathcal{F}(\varepsilon; J)}{\partial J}, \quad (3)$$

where

$$\mathcal{F}(\varepsilon; J) = N(\varepsilon, J) \langle \Delta J \rangle - \frac{1}{2} \frac{\partial}{\partial J} N(\varepsilon, J) \langle \Delta J^2 \rangle. \quad (4)$$

The diffusion coefficients $\langle \Delta J \rangle$ and $\langle \Delta J^2 \rangle$ obey the relation

$$\langle \Delta J^2 \rangle = 2J \langle \Delta J \rangle \quad (J \ll J_m), \quad (5)$$

(Lightman & Shapiro 1977; Magorrian & Tremaine 1999). Much of the difficulty in obtaining an exact solution for the Fokker-Planck equation stems from the dependence of the diffusion coefficients on the DF; self-consistency requires solving a set of coupled equations. For many practical applications the diffusion coefficients are estimated in a non-self-consistent way, for example by assuming homogeneity and isotropy (e.g. Binney & Tremaine 1987). Irrespective of its exact form, $\langle \Delta J^2 \rangle$ describes a random-walk process, and is therefore closely related to the relaxation time. In anticipation of the eventual necessity of introducing such approximations, we forgo from the outset the attempt to write down explicit expressions for the diffusion coefficients. Instead, we use them

¹ We use the notation $N(x; y)$, where x stands for any argument or set of arguments (scalar of vector) and y is a parameter, to denote the stellar number density per dx interval at y . The units of N are the inverse of those of x . For example, $N(\varepsilon; t) = \int_0^{J_m} dJ N(\varepsilon, J; t)$ is the stellar number density per unit specific energy at time t .

to *define* the relaxation time t_r as the time required to diffuse in J^2 by J_m^2 ,

$$t_r(\varepsilon) = \frac{J_m^2(\varepsilon)}{\langle \Delta J^2 \rangle}. \quad (6)$$

We then treat the relaxation time as a free parameter that characterizes the system's typical timescale for the evolution of the DF, and whose value can be estimated by Eqs. (25, 26) below. For simplicity, the relaxation time t_r is assumed to be independent of angular momentum², but can generally be a function of energy.

At steady state, the stellar current $\mathcal{F}(\varepsilon)$ is independent of J ,

$$\mathcal{F}(\varepsilon) = \frac{1}{2} \frac{J_m^2(\varepsilon)}{t_r} \left[\frac{N(\varepsilon, J)}{J} - \frac{\partial N(\varepsilon, J)}{\partial J} \right]. \quad (7)$$

Solving this equation yields

$$N(\varepsilon, J) = -\frac{2\mathcal{F}t_r}{J_m(\varepsilon)^2} J \ln J + C J. \quad (8)$$

The integration constants C and \mathcal{F} that are determined by the boundary conditions $N(\varepsilon, J_{lc}) = 0$ and $N(\varepsilon, J_m) = N_{\text{iso}}(\varepsilon, J_m)$. The isotropic DF is separable in ε and J ,

$$N_{\text{iso}}(\varepsilon, J) d\varepsilon dJ = \frac{2N_{\text{iso}}(\varepsilon)J}{J_m^2(\varepsilon)} d\varepsilon dJ. \quad (9)$$

Applying these boundary conditions³ to equation (8), the DF is given by

$$N(\varepsilon, J) = \frac{2N_{\text{iso}}(\varepsilon)J}{J_m^2(\varepsilon)} \frac{\ln(J/J_{lc})}{\ln(J_m/J_{lc})}, \quad (10)$$

and the stellar current into the MBH per energy interval is

$$\mathcal{F}(\varepsilon) = \frac{N_{\text{iso}}(\varepsilon)}{\ln(J_m/J_{lc})t_r(\varepsilon)}. \quad (11)$$

Note that the capture rate in the diffusive regime depends only logarithmically on the size of the loss cone.

The prompt infall rate Γ_p in the diffusive regime is then given by

$$\Gamma_p = \int_{\varepsilon_p}^{\infty} \frac{d\varepsilon N_{\text{iso}}(\varepsilon)}{\ln(J_m/J_{lc})t_r(\varepsilon)}, \quad (12)$$

where the energy ε_p separates the diffusive and full loss-cone regimes. A star samples all angular momenta $J_{lc} < J < J_m$ in a relaxation time, and it is promptly captured once $J < J_{lc}$. The total rate is therefore of order $\Gamma_p \sim N_{\text{iso}}(< a_p)/t_r(a_p)$, where a_p is the typical radius associated with orbits of energy ε_p (a_p is the semi-major axis for Keplerian orbits, see §2.2) and $N_{\text{iso}}(< a_p)$ is the number of stars within a_p . The rate is logarithmically suppressed because of the diluted occupation of phase space near the loss cone.

² In general, if the relaxation time depends on r , this will introduce some dependence of t_r on J . We do not consider this dependence here.

³ Adiabatic MBH growth may lead to some anisotropy (Quinlan, Hernquist & Sigurdsson 1995.). Here we assume that far from the loss-cone the DF will be isotropic

2.2. Keplerian orbits in a power-law cusp

The MBH dominates the stellar potential within the radius of influence,

$$r_h = \frac{GM_{\bullet}}{\sigma^2}, \quad (13)$$

where σ^2 is the 1D stellar velocity dispersion far from the MBH. The mass enclosed within r_h is roughly equal to M_{\bullet} . Various formation scenarios predict that the spatial stellar number density at $r < r_h$ should be approximately a power law (e.g. Bahcall & Wolf 1976; Young 1980)

$$n_{\star}(r) = \frac{(3/2 - p)N_h}{4\pi r_h^3} \left(\frac{r}{r_h} \right)^{-3/2-p}, \quad (14)$$

where N_h is the number of stars inside r_h . This corresponds to an energy distribution $N(\varepsilon)d\varepsilon \propto \varepsilon^{p-5/2}d\varepsilon$. A stellar cusp with $p \sim 0$ has been observed in the Galactic Center (Alexander 1999; Genzel et al. 2003). For a single mass population, it was shown by analytical considerations that $p = 1/4$ (Bahcall & Wolf 1976). This has been confirmed recently by N-body simulations (Baumgardt et al. 2004a; Preto et al. 2004).

Mass segregation drives the heavy stars in the population to the center. The radial distribution of the different mass components can be then approximated as average power-laws, steeper ($p > 0$) for the heavier masses and flatter ($p \lesssim 0$) for the lower masses (Bahcall & Wolf 1977; Baumgardt et al. 2004b).

Typically, the diffusive regime is within the radius of influence. We therefore assume from this point on that the stars move on Keplerian orbits ($\psi = GM_{\bullet}/r$) in a power-law density cusp. The stellar orbits are characterized by a semi-major axis a , eccentricity e , periapse r_p and period P ,

$$\begin{aligned} a &= \frac{GM_{\bullet}}{2\varepsilon}, & e^2 &= 1 - \frac{J^2}{GM_{\bullet}a}, \\ r_p &= a(1 - e), & P &= \frac{2\pi a^{3/2}}{\sqrt{GM_{\bullet}}}. \end{aligned} \quad (15)$$

During most of the inspiral $1 - e \ll 1$, and the periapse can be approximated by $r_p \approx J^2/2GM_{\bullet}$. This remains valid until the last phases of the inspiral.

The prompt infall rate (Eq. 12) can be expressed in terms of the maximal semi-major axis,

$$\Gamma_p = \int_0^{a_p} \frac{da N_{\text{iso}}(a)}{\ln(J_m/J_{lc})t_r(a)}. \quad (16)$$

We will assume Keplerian orbits throughout most of this paper except for section (4.1), where we employ the general relativistic potential of the MBH.

2.3. Slow inspiral

The derivations of the conditions necessary for slow inspiral and of the inspiral rate follow closely those of prompt infall, but with two important differences. (1) The time to complete the inspiral is not the infall time P_0 , but rather $t_0 \gg P_0$. (2) There is no contribution from the full loss-cone regime, where stars are scattered multiple times each orbit. This is because inspiral in this regime would require that the *very same* star that was initially deflected into an eccentric orbit, be re-scattered back into it multiple times. The probability for this

happening is effectively zero⁴.

In analogy to the radial scale a_p of prompt infall, which delimits the volume where stars can avoid scattering for a time $P_0 < t_J$, and thus maintain their infall orbit until they reach the MBH, the inspiral criterion $t_0 < t_J$ defines a critical radius $a_c \ll a_p$ (or equivalently, a critical energy $\varepsilon_c \gg \varepsilon_p$). Stars starting the inspiral from orbits with $a_0 < a_c$ ($\varepsilon_0 > \varepsilon_c$) will complete it with high probability, whereas stars starting with $a_0 > a_c$ ($\varepsilon_0 < \varepsilon_c$), will sample all J values before they spiral in significantly, *regardless of J_0* and ultimately either (1) fall in the MBH, (2) diffuse in energy to much wider orbits or (3) into the much tighter orbits of the diffusive regime. Since we assume a steady state DF, outcomes (2) and (3) represent a trivial, DF-preserving redistribution of stars in phase space, which does not affect the statistical properties of the system. Whether stars spiral in or fall in depends, statistically, only on a_0 (ε_0). We use below Monte Carlo simulations (§4.1, Fig. 3) to estimate the inspiral probability function, $S(a_0)$, which describes the probability of completing inspiral when starting from an orbit with semi-major axis a_0 ($S \rightarrow 1$ for $a_0 \ll a_c$, $S \rightarrow 0$ for $a_0 \gg a_c$). The inspiral rate for stars of type s with number fraction f_s is then

$$\Gamma_i = f_s \int_0^\infty \frac{daN(a)S(a)}{\ln(J_m/J_{lc})t_r(a)} \simeq f_s \int_0^{a_c} \frac{daN(a)}{\ln(J_m/J_{lc})t_r(a)}, \quad (17)$$

where roughly $S(a_c) \sim 0.5$.

3. PARAMETER DEPENDENCE OF THE INSPIRAL RATE

In this section we derive some analytical results for the inspiral rate. In order to keep the arguments transparent, we neglect relativistic deviations from Keplerian motion. Relativistic orbits are discussed in section (4.1).

Consider a star of mass M_* orbiting a MBH of mass M_\bullet on a bound Keplerian orbit with semi-major axis a and angular momentum J . When the star arrives at periape, it loses some orbital energy ΔE by GW emission. As a result, the orbit shrinks and its energy increases. For highly eccentric orbits the periape of the star is approximately constant during inspiral in absence of scattering. We define the inspiral time t_0 as the time it takes the initial energy ε_0 to grow formally to infinity. If the energy loss per orbit is constant, then for $e \rightarrow 1$

$$t_0 = \int_{\varepsilon_0}^\infty \frac{d\varepsilon}{(d\varepsilon/dt)} \approx \frac{1}{\Delta E} \int_{\varepsilon_0}^\infty d\varepsilon P(\varepsilon) = \frac{2\varepsilon_0 P_0}{\Delta E}, \quad (18)$$

or

$$t_0(r_p, a) = \frac{2\pi\sqrt{GM_\bullet a}}{\Delta E}. \quad (19)$$

For GW, ΔE is given by (Peters 1964)

$$\Delta E_{\text{GW}} = \frac{8\pi}{5\sqrt{2}} f(e) \frac{M_* c^2}{M_\bullet} \left(\frac{r_p}{r_S}\right)^{-7/2}, \quad (20)$$

where

$$f(e) = \frac{1 + \frac{73}{24}e^2 + \frac{37}{96}e^4}{(1+e)^{7/2}}, \quad (21)$$

and $r_S = 2GM_\bullet c^2$ is the Schwarzschild radius.

⁴ This is to be contrasted with prompt infall from the full loss-cone regime, where a star can reach the MBH by being scattered *once* into the loss-cone just before crossing a_p toward the MBH.

During all but the last stages of the inspiral $e \sim 1$, in which case $r_p/r_S = 4(J/J_{lc})^2$ and

$$\Delta E_{\text{GW}} = E_1 (J/J_{lc})^{-7}, \quad E_1 \equiv \frac{85\pi}{3 \times 2^{13}} \frac{M_* c^2}{M_\bullet}. \quad (22)$$

Gravity waves also carry angular momentum,

$$\Delta J_{\text{GW}} = -\frac{16\pi}{5} g(e) \frac{GM_*}{c} \left(\frac{r_p}{r_S}\right)^{-2}, \quad (23)$$

$$g(e) = \frac{1 + \frac{7}{8}e^2}{(1+e)^2}. \quad (24)$$

Generally, the change in J in the course of inspiral is dominated by two-body scattering, and ΔJ_{GW} can be neglected until a becomes very small.

It is convenient to refer the timescales in the system to the relaxation time at the MBH radius of influence,

$$t_h = A_p \left(\frac{M_\bullet}{M_*}\right)^2 \frac{P(r_h)}{N_h \log \Lambda_1}, \quad (25)$$

where $\Lambda_1 = M_\bullet/M_*$ (r_S/r_h)^{1/4} (Miralda-Escudé & Gould 2000), and $A_p \simeq 0.2$ for $p=0$ (Alexander & Hopman 2003). The relaxation time at any radius is then

$$t_r(a) = t_h \left(\frac{a}{r_h}\right)^p, \quad (26)$$

where we associate the typical relaxation time on an orbit with that at its semi-major axis. This is a good approximation, since theoretical arguments (Bahcall & Wolf 1976; 1977) and simulations (Freitag & Benz 2002; Baumgardt et al. 2004a 2004b; Preto et al. 2004) indicate that $0 \lesssim p \lesssim 0.25$, and so t_r is roughly independent of radius. The angular momentum relaxation time is

$$t_J = \left[\frac{J}{J_m(a)}\right]^2 \left(\frac{a}{r_h}\right)^p t_h. \quad (27)$$

Dissipational inspiral takes place in the presence of two-body scattering. When $t_0 \sim t_J$, both effects have to be taken into account. It is useful to parametrize the relative importance of dissipation and scattering by the dimensionless quantity

$$s(J, a) \equiv \frac{t_0(J, a)}{t_J(J, a)} = \left(\frac{a}{d_c}\right)^{3/2} \left(\frac{a}{r_h}\right)^{-p} \left(\frac{J}{J_{lc}}\right)^5, \quad (28)$$

where we introduce the (p -independent) length scale

$$d_c \equiv \left(\frac{8\sqrt{GM_\bullet} E_1 t_h}{\pi c^2}\right)^{2/3}, \quad (29)$$

which is of the same order as a_c (Eq. 30) and is $\ll r_h$. We define some critical value $s_{\text{crit}} \ll 1$ such that the inspiral is so rapid that the orbit is effectively decoupled from the perturbations.

The three phases of inspiral can be classified by the value of s . In the ‘‘scattering phase’’ the star is far from the region in phase space where GW emission is efficient and $s \gg 1$. With time it may scatter to a lower- J orbit, enter the ‘‘transition phase’’, where $s \sim 1$, and start to spiral in. If it is not scattered into the MBH or to a wide orbit, it will eventually

reach the stage where $s < s_{\text{crit}}$. It will then enter the “dissipation phase” where it spirals-in deterministically according to equations (20–24). Note that eventually the $e \rightarrow 1$ approximation is no longer valid.

Here we are mainly interested in understanding how the interplay between two-body scattering and energy dissipation in the first two phases sets the initial conditions for the GW emission in the final phase. It should be emphasized that the onset of the dissipation phase does not necessarily coincide with the emission of *detectable* GW. For example, while a star is well into the dissipation phase by the time $s < s_{\text{crit}} \sim 10^{-3}$, the orbit has still to decay substantially before the GW frequency becomes high enough to be detected by *LISA*.

We derive an analytical order of magnitude estimate for the critical semi-major axis a_c by associating it with $s = 1$ orbits in the transition phase. Since s falls steeply with J , we set $J = J_{lc}$ and solve $s(J_{lc}, a_c) = 1$ for a_c , obtaining

$$\frac{a_c}{r_h} = \left(\frac{d_c}{r_h} \right)^{3/(3-2p)}. \quad (30)$$

The MC simulations below (§4.1) confirm that this analytical estimate corresponds within a factor of order unity to the semi-major axis where the inspiral probability $S(a_c) \sim 0.5$, for a wide range of masses (see table [2]). Expression (17) for the rate can then be approximated by

$$\Gamma_i \sim \frac{f_s N_h}{t_h \ln[J_m(a_c)/J_{lc}]} \left(\frac{a_c}{r_h} \right)^{3/2-2p}, \quad (31)$$

where N_h is the number of stars within r_h .

The dependence of the inspiral rate on p (at fixed d_c/r_h and neglecting the logarithmic terms) can be examined by writing $\Gamma_i \simeq g(p) f_s (N_h/t_h)$, where

$$g(p) = \left(\frac{d_c}{r_h} \right)^{3(3-4p)/2(3-2p)}. \quad (32)$$

The pre-factor $g(p)$ grows with p over the relevant range (see also Ivanov 2002). This reflects the fact that the inspiral rate is determined by the number of stars within a_c , rather than the total number of stars within r_h . The concentration of the cusp increases with p , so that there are more stars within a_c . This result suggests qualitatively that in a mass-segregated population, the heavier stars (higher p) will have an enhanced GW event rate compared to the light stars (lower p).

From equations (29–32) it follows that

$$\Gamma_i \propto t_h^{-2p/(3-2p)}. \quad (33)$$

Since $p \sim 0$ for typical stellar cusps around MBHs, this means that the inspiral rate is nearly independent of the relaxation time for such cusps. This counter-intuitive result reflects the near balance between two competing effects. When scattering is more efficient, stars are supplied to inspiral orbits at a higher rate, but are also scattered off them prematurely at a higher rate, so the volume of the diffusive regime, which contributes stars to the inspiral ($\sim a_c^3$), decreases. This is in contrast to the prompt disruption rate Γ_p , which increases as the relaxation time becomes shorter⁵. It then follows that enhanced scattering, such as by massive perturbers (e.g. clusters, giant molecular clouds; Zhao, Haehnelt & Rees 2002)

⁵ The prompt disruption rate is $\Gamma_p \sim N(<a_p)(r_S/a_p)/P(a_p)$ (Syer & Ulmer 1999, Eq. 10). For prompt disruption $a_p \sim t_h^{2/(5-2p)}$ (Alexander & Hopman 2003), and so the rate scales as $\Gamma_p \sim t_h^{-(2+2p)/(5-2p)}$.

increases the prompt disruption rate, but will not enhance the rate of inspiral events.

The dependence of the GW event rate on the mass of the MBH can be estimated from Eq. (31) and the empirical M_\bullet – σ relation

$$M_\bullet = 1.3 \times 10^8 M_\odot \left(\frac{\sigma}{200 \text{ km s}^{-1}} \right)^\beta, \quad (34)$$

where $\beta \sim 4$ (Ferrarese & Merritt 2000; Gebhardt et al. 2000; Tremaine et al. 2002). Note that the M_\bullet – σ relation implies that the stellar number density at the radius of influence, n_h is larger for lighter MBHs: for example, for $\beta = 4$, $n_h \propto N_h r_h^{-3} \propto M_\bullet^{-1/2}$, where we assumed that $N_h \propto M_\bullet$; the consequences of this for the dependence of the rate for prompt tidal disruptions on the MBH mass were discussed by Wang & Merritt (2004).

The GW event rate depends on M_\bullet as

$$\Gamma_i \propto M_\bullet^{3/\beta-1}. \quad (35)$$

This dependence is weak, e.g. $\Gamma_i \propto M_\bullet^{-1/4}$ for $\beta = 4$. Thus, the rate becomes *higher* for lower mass MBHs. If $M_\bullet \sim 10^3 M_\odot$ IBHs indeed exist in stellar clusters and the M_\bullet – σ relation can be extrapolated to these masses, then they may be more likely to capture stars than MBHs. This, however, does not necessarily translate into more GW sources. The strain h of GW decreases with the mass of the MBH, so that these sources have to be closer by in order to observe their GW emission. Another restriction is that for IBHs the tidal force is so strong that white dwarfs are tidally disrupted well outside the event horizon, which precludes them from being *LISA* sources. These issues are further discussed in §5.

4. ORBITAL EVOLUTION WITH DISSIPATION AND SCATTERING

We present three different methods for analyzing inspiral in the presence of scattering. The first approach is based on Monte Carlo (MC) simulations, which follow a star on a relativistic orbit, described by ε and J , and add small perturbations to simulate energy dissipation and random two-body scattering. The second approach consists of direct numerical integration of the time dependent diffusion-dissipation equation. The third approach is a heuristic semi-analytical effective model that can describe the “effective” trajectory of a star through phase space, as well as the statistical properties of an ensemble of such trajectories.

The three approaches are complementary. The MC simulations allow a direct realization of the micro-physics of the system, since they follow the perturbed orbits of individual stars. They also offer much flexibility in setting the initial conditions of the numerical experiments, but the results are subject to statistical noise and are not easy to generalize. The diffusion-dissipation equation on the other hand deals directly with the DF, and allows an analytical formulation of the problem in terms of partial differential equations, which are solved numerically. However, computational limitations do not allow covering as large a dynamical range as in the MC simulations. Finally, the heuristic effective model has the advantage of its intuitive directness and relative simplicity of use. We find that all three methods give the same results for the same underlying assumptions (Fig. 2). This inspires confidence in the robustness of the analysis.

To compare the three methods, we stop the simulation at the point where $s = s_{\text{crit}} = 10^{-3}$, and we plot the DF of the angular momenta of the stars. From that point on the stars

are effectively decoupled from the cluster and can spiral in undisturbed. We then use the MC method, which can be easily extended to follow the stars in the dissipation phase (section 5), to find the DF of the eccentricities of stars which enter the *LISA* band.

4.1. Monte Carlo simulations

The MC simulations generally follow the scheme used by Hills & Bender (1995) to study the event rate of GW. The star starts on an initial orbit with (ε_0, J_0) such that dissipation by GW emission is negligible. The initial value of J is not of importance as the angular momentum is quickly randomized in the first few steps of the simulation. Every orbital period $P(\varepsilon)$, the energy and angular momentum are modified by $\delta\varepsilon$ and δJ , and the orbital period and periaapse are recalculated (this diffusion approach is justified as long as $P \ll t_J$). The simulation stops when the star decays to an orbit with $s < s_{\text{crit}} = 10^{-3}$ or when $J < J_{lc}$ and it falls in the MBH (escape to a less bound orbit is not an option here since energy relaxation is neglected and only dissipation is considered; see §2.3).

When stars reach high eccentricities as a result of scattering, the periaapse approaches the Schwarzschild radius to the point where the Newtonian approximation breaks down. The MC simulations take this into account by integrating the orbits in the relativistic potential of a Schwarzschild MBH. The periaapse of the star moving in a Schwarzschild spacetime is related to its angular momentum by one of the three roots of the equation

$$E_{\text{GR}}^2 = \left(c^2 - \frac{2GM_\bullet}{r} \right) \left(c^2 + \frac{J^2}{r^2} \right) \equiv V_{\text{GR}}(r, J). \quad (36)$$

The term on left hand side of this equation is the squared specific relativistic energy of the star (including its rest mass), while the right hand side is the effective GR potential. A star on a bound orbit is not captured by the MBH as long as equation (36) has three real roots for r . The smallest root is irrelevant for our purposes. The intermediate root (the turning-point) is the periaapse r_p of the orbit, and the largest root is the apo-apse r_a . The semi-major axis a and eccentricity e are defined by $a = (r_p + r_a)/2$ and $e = 1 - r_p/a$ (see Eq. 15). For bound orbits the loss cone J_{lc} is a very weak function of energy and is well approximated by Eq. (1).

For given values of E and J , the GR periaapse is smaller than the Newtonian one, and therefore the orbits can be more eccentric, and the dissipation can be stronger than implied by the Newtonian approximation. The Keplerian relations between energy, angular momentum and the orbital parameters (Eqs 15) are replaced by

$$E_{\text{GR}}^2 = \frac{(q - 2 - 2e)(q - 2 + 2e)}{q(q - 3 - e^2)}; \quad (37)$$

$$J^2 = \frac{q^2}{q - 3 - e^2} \left(\frac{GM_\bullet}{c} \right)^2, \quad (38)$$

where $q = 2(1 - e^2)a/r_S$ (Cutler, Kennefick & Poisson 1994). The condition for a non-plunging orbit can also be expressed in terms of the eccentricity and the semi-major axis, $2(1 - e^2)a = (6 + 2e)r_S$ (Cutler et al. 1994). This corresponds to a maximal eccentricity for a star on a non-plunging orbit

$$e_{\text{max}}(a) = -\frac{r_S}{2a} + \sqrt{(r_S/2a)^2 - 3r_S/a + 1}, \quad (39)$$

which increases with a . If $a_L = (P_L^2/4\pi^2 GM_\bullet)^{1/3}$ is the maximal semi-major axis a star may have in order to be detectable by *LISA*, the maximal eccentricity of a star detectable by *LISA* is $e_{\text{max}}(a_L)$.

The step in J -space per orbit is the sum of three terms

$$\delta J(\varepsilon, J) = \Delta_1 J_{\text{scat}}(\varepsilon, J) + \chi \Delta_2 J_{\text{scat}}(\varepsilon, J) - \Delta J_{\text{GW}}(\varepsilon, J). \quad (40)$$

The first and second terms represent two-body scattering (Eqs. 2,5,6), with⁶ $\Delta_1 J_{\text{scat}} = \langle \Delta J \rangle P = J_m^2 P(\varepsilon)/(2t_r J)$ and $\Delta_2 J_{\text{scat}} = \sqrt{\langle \Delta J^2 \rangle P} = \sqrt{P(\varepsilon)/t_r J_m(\varepsilon)} = \sqrt{P(\varepsilon)/t_r J}$. The random variable χ takes the values ± 1 with equal probabilities. The third term is the deterministic angular momentum loss due to GW emission (Eq. 23). The energy step per orbit is deterministic (diffusion in energy is neglected)

$$\delta E(\varepsilon, J) = \Delta E_{\text{GW}}(\varepsilon, J). \quad (41)$$

In order to increase the speed of the simulation we use an adaptive time-step. We checked for some cases that taking a smaller time-step does not affect the results.

The DF of inspiraling stars is generated by running many simulations (typically 3×10^4) of stellar trajectories through phase space with the same initial value for J_0 , but different random perturbations. We record the fraction of stars that avoid falling in the MBH, $S(a_0)$, and the value of J at s_{crit} for those stars that reach the dissipation-dominated phase, thereby obtaining the DF $W(J; a_0)$. This is repeated for a range of a_0 values. The integrated DF over all cusp stars, $W(J)$, is then obtained by taking the average of all DFs, weighted by $N(a_0)S(a_0)da_0$ (cf Eq. 17).

4.2. Diffusion equation with GW dissipation

The DF of the inspiraling stars at the onset of the dissipation dominated phase can be obtained directly by solving the diffusion-dissipation equation. This approach was taken by Ivanov (2002), who included a GW dissipation term and obtained analytic expressions for the GW event rate for $J \gg J_{lc}$ under various simplifying assumptions. Here we are interested DF of stars very near the loss-cone, and so we integrate the diffusion-dissipation equation numerically with two simplifying assumptions. (1) We neglect the drift term in the diffusion-dissipation equation. This can be justified by noting that the drift grows linearly with time, $\delta J_1(t) = J_m^2 t/(2t_r J)$, while the change due to the random walk grows as $\delta J_2(t) = (t/t_r)^{1/2} J_m$. For a star with initial angular momentum J the drift becomes important only for $t > t_{\text{drift}} = 4(J/J_m)^2 t_r = 4t_J$. Since we are interested in the timescales $t \sim t_0 \leq t_J$, the drift is only a small correction. (2) We assume Keplerian orbits. These approximations are validated by the very good agreement with the MC simulation results (section 4.4).

With these two assumptions, the diffusion-dissipation is (cf Eqs. 3, 7)

$$\frac{\partial N(\varepsilon, J; t)}{\partial t} = \frac{J_m^2(\varepsilon)}{2t_r} \frac{\partial^2}{\partial J^2} N(\varepsilon, J; t) + \frac{\partial}{\partial \varepsilon} \left[\dot{E}_{\text{GW}}(J) N(\varepsilon, J; t) \right], \quad (42)$$

⁶ The drift term $\Delta_1 J_{\text{scat}}$ represents a bias to scatter *away* from the MBH due to the 2D character of the direction of the velocity vector \mathbf{v} . This can be expressed geometrically by considering a circle of radius Δv_{scat} centered on \mathbf{v} ($\mathbf{v} + \Delta \mathbf{v}_{\text{scat}}$ is the change per orbit due to scattering). This circle is intersected by a second circle of radius v that passes through \mathbf{v} and is centered on the radius vector to the MBH. The section of the first circle that leads away from the MBH is slightly larger than the section leading toward it.

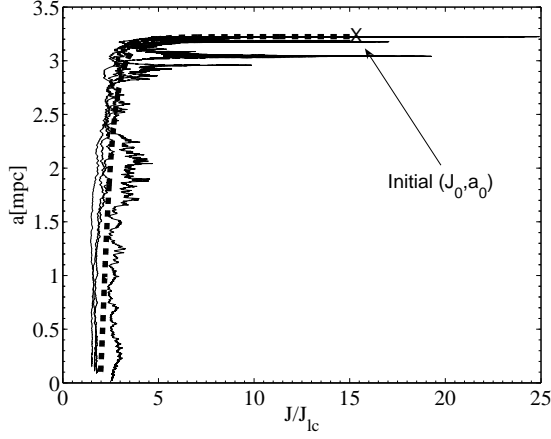


FIG. 1.— Examples of tracks of stars from the MC simulation (solid lines), and a track from the effective model (dashed line) with $\xi = 1$. The effective track represents the stochastic tracks well. The tracks extend to the point where $s = 10^{-3}$. The relevant parameters are given in the first line of table (2), i.e. inspiral of a white dwarf into a MBH.

where $\dot{E}_{\text{GW}} = \Delta E_{\text{GW}}/P$ is the rate at which energy is lost to GW. The first term accounts for diffusion in J -space and the second represents the energy dissipated by GW emission. As with the MC simulations, the diffusion coefficient $\langle \Delta J^2 \rangle = J_m^2/t_r$ is an input parameter rather than resulting from a self-consistent calculation.

The initial conditions consist of an isotropic cusp DF, $N(\varepsilon, J) \propto \varepsilon^{p-5/2} J$ and the boundary condition that the DF vanish on the loci $s = s_{\text{crit}} = 10^{-3}$ and $J = J_{lc}$ in the (ε, J) -grid. The initial DF is evolved in time over the (ε, J) -grid until $t \sim t_J$, when a relaxed steady state is achieved. The integration is done using a Forward Time Centered Space (FTCS) representation of the diffusion term, and an ‘upwind’ differential scheme for the dissipation term (see e.g. Press et al. 1992). After each time step (which are chosen small enough to obey the Courant condition) the DF is re-normalized so that captured stars are replenished.

After relaxation, the DF is non-zero up to the boundary $s = s_{\text{crit}}$, as stars are redistributed in phase space by diffusion at large J and by dissipation at small J . The DF at s_{crit} is then extracted to construct the angular momentum DF, $W(J)$. Although the stars continue their trajectory in phase space beyond s_{crit} all the way to the last stable orbit, this does not change $W(J)$ because the rapid energy dissipation does not allow much J -diffusion.

4.3. Analytical model of effective orbit

Stars follow complicated stochastic tracks in (J, a) space; due to scattering they move back and forth in J , while they always drift to smaller a due to GW dissipation (energy diffusion by scattering is neglected). The drift rate depends strongly on J . Figure (1) shows some examples of stellar tracks in phase space, taken from the MC simulations.

In this section we propose a heuristic analytical model, which captures some essential results of the MC simulations, while providing a more intuitive understanding.

In this model we define the equations of motion of an ‘effective track’ of a star, which is deterministic and can be solved analytically. With this method we follow stars that start at some given initial semi-major axis a_0 and angular momentum J_0 , and follow the star during its first two stages of

inspiral, i.e., until the moment that $s < s_{\text{crit}}$.

The DF of stars which reach $s = s_{\text{crit}}$ is determined by the evolution of the orbital parameters (J, a) in the region where energy dissipation is efficient. Because of the strong dependence of the energy ΔE which is dissipated per orbit on angular momentum (or, equivalently, periaapse), this is a small region ΔJ in J -space, the size of which is of order of the loss-cone, $\Delta J \sim J_{lc}$. The time Δt it typically takes a star with semi-major axis a_0 performing a random walk in J to cross this region is $\Delta t = [\Delta J/J_m(a_0)]^2 t_h$ ($t_r = t_h$ assumed). This can be used to introduce an effective J -‘velocity’ $\Delta J/\Delta t = -J_m^2(a_0)/J_{lc} t_h$.

The effective velocity of the semi-major axis is given by

$$\frac{da(J, a)}{dt} = \frac{da}{dE} \dot{E} = -\frac{2a^2}{GM_\bullet} \frac{\Delta E_{\text{GW}}(J)}{P(a)}. \quad (43)$$

These two equations define a deterministic time evolution in (J, a) space from given initial values $(J(0) = J_0, a(0) = a_0)$, to a final point (J_f, a_f) , where $s = s_{\text{crit}}$. To recover $W(J; a_0)$ at s_{crit} , we introduce some scatter in the effective velocities dJ/dt ,

$$\frac{dj}{dt} = -\xi y \frac{j_c^2(a_0)}{t_h}, \quad (44)$$

where j denotes angular momentum in terms of J_{lc} , y is drawn from the positive wing of the normalized Gaussian distribution, $G_1(y)$, and $\xi \sim 1$ (a free parameter) is the width of the distribution, which can vary depending on the system’s parameters. Equations (43,44) can be solved analytically,

$$j(t) = j_0 - y \xi j_c^2(a_0) \frac{t}{t_h}, \quad a(t) = \left[1 - \frac{(d_c/a_0)^{3/2}}{6 \xi y j^6} \right]^2 a_0. \quad (45)$$

The stopping condition $s(j, a) = s_{\text{crit}}$ gives an additional relation between j and a , so that the final values are related by $a_f = s_{\text{crit}}^{2/3} j_f^{-10/3} d_c$. This ties the initial and final values through the equations of motions

$$y(j_f) = \frac{(6\xi)^{-1} (d_c/a_0)^{3/2} j_f^{-6}}{1 - s_{\text{crit}}^{1/3} (d_c/a_0)^{1/2} j_f^{-5/3}}. \quad (46)$$

The relation between the initial distribution of j -velocities and the final j distribution at is $W(j_f; a_0) = G_1(y)[dy(j_f)/dj_f]$. The integrated DF over all the cusp stars is

$$W(j_f) dj_f = \frac{\int^{a_c} N(a) W(j_f; a) da}{\int^{a_c} N(a) da}. \quad (47)$$

4.4. Comparison of the different methods

We compare the results of the MC simulation, the diffusion-dissipation equation and an integration of equations (44) and (43). In all cases the calculation is stopped when $s = 10^{-3}$; at that point the eccentricity is still approximately unity, but scattering becomes entirely negligible so that even in the MC simulation the quantities evolve essentially deterministically according to equations (20-24). The calculations assume a cusp with slope $p = 0$, $M_\bullet = 3 \times 10^6 M_\odot$ and $M_\star = 0.6$ (corresponding to WDs).

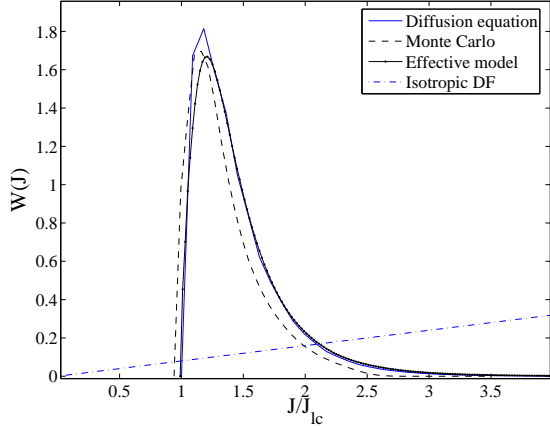


FIG. 2.— A comparison of the DFs of angular momenta for inspiraling stars in a $p=0$ stellar cusp, derived from (1) MC simulations, (2) direct integration of the diffusion-dissipation equation (Eq. 42) and (3) the effective model (Eq. 47, with $\xi=0.6$). The DFs are normalized over the displayed J -range. The DFs are shown at $s=10^{-3}$, when the dynamics are dominated by dissipation and scattering no longer plays a role, but the orbits are still well outside the *LISA* band, $P \gg P_L$ and $e \rightarrow 1$. This DF sets the initial conditions for the dissipation phase. The DF of the isotropic parent population (no sink, no dissipation; Eq. 9) is also shown for contrast. Unlike the DF of the inspiraling stars, it is dominated by high- J stars.

TABLE 1
COMPARISON OF ASSUMPTIONS IN THE 3 METHODS

Method	GR potential	$\Delta_1 J_{\text{scat}}$	ΔJ_{GW}	Stop at s_{crit}
Monte Carlo	yes	yes	yes	no ^a
Diffusion/Dissipation	no	no	no	yes
Effective track	no	no	no	yes

^a For the purpose of comparison to the other two methods, the MC simulation was terminated at s_{crit} .

Figure (2) shows the very good correspondence between the three approaches, whose underlying assumptions and approximations are summarized in table (1). One important conclusion is that all stars enter the dissipation phase with very small angular momenta, $1 \lesssim J/J_{lc} \lesssim 2$. For a suitable choice of $\xi \sim 1$, the actual complicated stochastic tracks are well mimicked by the tracks of the “effective stars”. The semi-analytical approach not only identifies the correct scale of angular momentum of inspiraling stars, but reproduces the DF. Its practical value lies in the relative ease of its application compared to the time consuming MC simulations or the integration of the diffusion-dissipation equation.

5. INSPIRAL RATES AND DISTRIBUTION OF ORBITAL PARAMETERS

We now proceed to apply the MC simulation to different types of COs inspiraling into a $3 \times 10^6 M_\odot$ MBH in a galactic center, and into a $10^3 M_\odot$ IBH in a stellar cluster. We find from the simulations the critical semi-major axis a_c and calculate the DF of the eccentricities of *LISA* sources. We stop the simulations when the orbital period falls below the longest period detectable by *LISA*, $P_L = 10^4$ s, which corresponds to a semi-major axis of

$$a_L = 23.5 M_6^{-2/3} r_S, \quad (48)$$

TABLE 2
PARAMETERS FOR STELLAR POPULATIONS AND INSPIRAL RATES

Star	M_* [M_\odot]	t_h [Gyr]	r_h [pc]	p	f_s	a_c^c [mpc]	a_c^d [mpc]	Γ_i [Gyr^{-1}]
WD ^a	0.6	10	2	0	0.1	30	20	7.8
NS ^a	1.4	5	2	0	0.01	40	20	1.8
BH ^a	10	1	2	1/4	1(-3)	20	10	4.7
NS ^b	1.4	1(-3)	0.05	0	0.01	2	1	4.3
BH ^b	10	1(-3)	0.05	1/4	1(-3)	5	2	6.7

^a MBH with $M_\bullet = 3 \times 10^6 M_\odot$
^b IBH with $M_\bullet = 10^3 M_\odot$.
^c From equation (30)
^d From the MC simulations

where $M_\bullet = 10^6 M_6 M_\odot$. We record the eccentricity at that point and construct the DF of the eccentricity at P_L . It is straightforward to integrate the orbits in the eccentricity histograms backward (forward) in time to larger (smaller) values of P , see e.g. Barack & Cutler (2003).

The stars are distributed according to a powerlaw distribution with different values for p . The total number of stars within r_h was assumed to be $N_h = 2M_\bullet/M_\odot$, with different number fractions for the respective species. See table (2) for the assumed parameters of the stellar populations.

5.1. Massive black holes in galactic centers

We assume a $M_\bullet = 3 \times 10^6 M_\odot$ MBH as a representative example and make the simplifying assumption that the MBH is not spinning. Real MBHs probably have non-zero angular momentum (e.g. see for evidence of spin of the MBH in our Galactic Center Genzel et al. 2003). An important qualitative difference is that in the Schwarzschild case the eccentricity of a GW-emitting star decreases monotonically with time, which is not so for non-zero angular momentum (e.g. Glampedakis et al. 2002). We conducted several MC simulations with Kerr metric orbits and verified that in spite of changes in details, our overall results hold.

The tidal field of MBHs in this mass range disrupts main sequence stars before they can become detectable *LISA* sources. A possible exception is our own Galactic Center, where the weak GW emission from very low mass main sequence stars (which are the densest and so the most robust against tidal disruption) may be detected because of their proximity (Freitag 2003). However, here we only consider GW from COs. Table (2) summarizes the parameters assumed for the properties of white dwarfs (WDs), neutron stars (NSs) and stellar mass black holes (BHs). The BHs are assumed to be strongly segregated in a steep cusp because of their much heavier mass (Bahcall & Wolf 1977). The total (dark) mass in COs near MBHs is not known, but in future it may be constrained by deviations from Keplerian motions of luminous stars very near the MBH in the Galactic center (Mouawad et al. 2004).

Fig. (3) shows the normalized inspiral probability function $S_s(a_0)$, where s stands for WD, NS, and BH. The critical semi-major axis is similar for WDs and NSs, but much smaller for BHs, because of the smaller relaxation time and the higher central concentration due to mass segregation. The functions $S_s(a)$ are used to calculate the inspiral rates (Eq. 17) that are listed in table (2). The rate for WDs is highest, $\Gamma_{\text{WD}} = 7.8 \text{ Gyr}^{-1}$. We find that because of mass segrega-

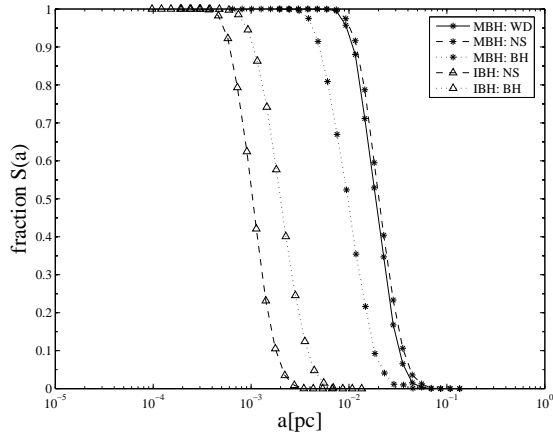


FIG. 3.— Dependence of the normalized fraction of inspiral events on initial semi-major axis, for the case of a MBH of $M_{\bullet} = 3 \times 10^6 M_{\odot}$ (asterisks) and an IBH (triangles). The solid line is for white dwarfs, the dashed lines for neutron stars, and the dotted lines for stellar mass black holes. For the parameters of these cases see table (2).

tion, the rate for stellar BHs is of the same order of magnitude as that for WDs, $\Gamma_{\text{BH}} = 4.7 \text{ Gyr}^{-1}$ although their number fraction is lower by two orders of magnitude. The hierarchy of rates in table (2) is not, of course, necessarily the same as cosmic rates that *LISA* will observe; NSs and BHs are more massive than WDs, and can be observed at larger distances.

Fig. (4) shows the eccentricity DFs of stars on orbits with $P = P_L$; note that since $a = a_L$ is fixed, the orbits are fully determined by e . The DFs show a strong bias to large eccentricities. The maximal eccentricity possible for a star orbiting a $3 \times 10^6 M_{\odot}$ MBH in the *LISA* band is $e_{\text{max}} = 0.81$ (Eq. 39).

It should be emphasized that the histogram in figure (4) can be obtained deterministically from the DF $W(J; s_{\text{crit}} = 10^{-3})$ in figure (2), because the stars have already reached the point where scattering is negligible. This would not be the case had the MC simulation been terminated at $s_{\text{crit}} = 1$ (e.g. Freitag 2003), since then significant scatterings would continue to redistribute the orbital parameters. We find however that the final DF (at $P = P_L$), which is obtained by integrating $W(J; s_{\text{crit}} = 1)$ forward in time according to the GW dissipation equations (Eqs. 20,23) without scattering, is not much different from that shown in Fig. (4). This coincidence is due to the fact that the stars with the largest eccentricities, which typically drop into the MBH, are replenished by the stars with slightly lower eccentricities. The main consequence of choosing s_{crit} too large is an overestimate of the total event rate; stars which actually fall into the MBH are erroneously counted as contributing to the GW event rate. Incidentally, even though stars that do not complete the inspiral are not individually resolvable, they will contribute to the background noise in the *LISA* band (Barack & Cutler 2004).

A premature neglect of the effects of scattering in previous studies (e.g. Freitag 2001) probably explains in part why our derived rates are significantly lower. Those studies usually assumed that stars will spiral without further perturbations once $s = 1$. We confirmed this by running a simulation that was stopped at $s_{\text{crit}} = 1$ instead of $s_{\text{crit}} = 10^{-3}$. We found that the event rate in that unrealistic case is about ~ 6 times higher. This may explain why our rates are lower than those estimated by Hills & Bender (1995), who used a method similar to ours, without specifying the criterion for inspiral.

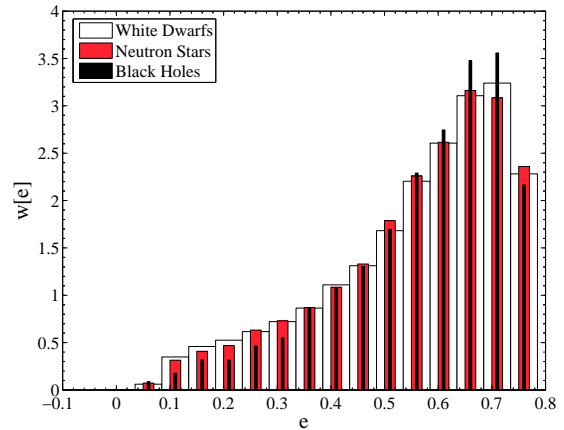


FIG. 4.— The probability DF of a CO entering the *LISA* band with eccentricity e for a MBH of mass $M_{\bullet} = 3 \times 10^6 M_{\odot}$. The histograms represent WDs, NSs and BH (from broad to narrow). Note that the maximal possible eccentricity for which $P < P_L$ is $e_{\text{max}} = 0.81$. See table (2) for the cusp parameters.

5.2. Intermediate mass black holes in stellar clusters

Unlike MBHs with masses $M_{\bullet} \gtrsim 10^6 M_{\odot}$, there is little firm observational evidence at this time for the existence of IBHs with masses $M_{\bullet} \sim 10^3 M_{\odot}$ (see review by Miller & Colbert 2004). However, there are plausible arguments arguing in favor of their existence. From a theoretical point of view, these objects are thought to form naturally, such as in population III remnants (Madau & Rees 2001), or in a runaway merger of young stars in dense stellar clusters (Portegies Zwart & McMillan 2001; Portegies Zwart et al. 2004). From an observational perspective, IBHs may power some of the ultraluminous X-ray sources (e.g. Miller, Fabian, & Miller 2004), for example by tidal capture of a main sequence companion star (Hopman et al. 2004).

For the purpose of estimating the orbital parameters of GW emitting stars, we assume that IBHs lie at the center of dense stellar clusters (see model parameters listed in table 2). White dwarfs are disrupted by an IBH before entering the *LISA* band, so that only the most compact sources, neutron stars and stellar mass BHs can emit GW in the *LISA* frequency band.

Figure (3) shows the inspiral probability functions $S_s(a)$, and Fig. (5) shows the eccentricity histograms of stars on orbits with $P = P_L$. The maximum eccentricity still observable by *LISA* is nearly unity, and the IBH case shows even more clearly the strong tendency towards large eccentricities. In general, this effect becomes more prominent for lighter BHs. The high eccentricity makes the GW signal highly non-monochromatic. The star spends most time at apo-apse, emitting a relatively weak, low frequency signal. At periape short pulses of high frequency GW is emitted. For IBHs of $M_{\bullet} \sim 10^3 M_{\odot}$, the frequency ν_p of these short bursts at periape is of the order $\nu_p \lesssim 100 \text{ Hz}$. This is too high to be measurable by *LISA*, but may be measurable by ground based detectors such as *LIGO* or *VIRGO*.

As anticipated (Eq. 35), the rate of inspiraling stars is comparable to that of a MBH (Table 2). However, due to the extremely high eccentricities and small semi-major axes of the orbits, the GW emission is very efficient and they spiral in on a very short time scale (on the order of a year).

6. SUMMARY AND DISCUSSION

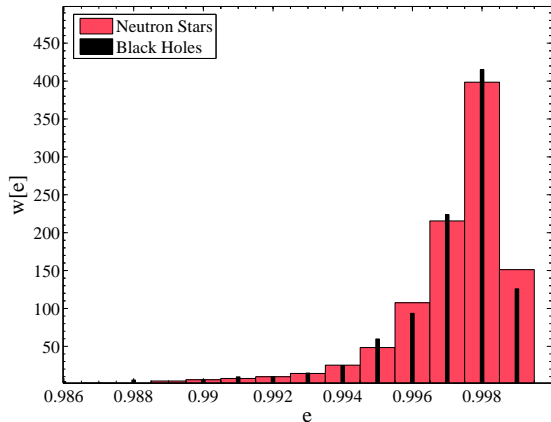


FIG. 5.— The probability DF of a compact remnant entering the *LISA* band with eccentricity e for an IBH of mass $M_\bullet = 10^3 M_\odot$. Only NSs (broad) and BHs (narrow) are considered; WDs are probably disrupted by the tidal field. For an IBH, the maximal possible eccentricity for which $P < P_L$ is nearly unity, $e_{\max} = 0.998$, all inspiraling stars are likely to have eccentricities close to the maximum value. See table (2) for the cusp parameters.

Stars spiraling into MBH due to the emission of GW are an important potential source for future GW detectors, such as *LISA*. The detection of the signal against the noise will be challenging, and requires pre-calculated wave-forms. The waveforms depend on the orbital parameters of the inspiraling stars. Our main goal in this study was to derive the distribution of eccentricities of inspiraling stars. The orbital statistics of such stars reflect a competition between orbital decay through dissipation by the emission of GW, and scattering, which deflects stars into eccentric orbits but can also deflect them back to wider orbits or straight into the MBH.

Inspiral is a slow process, and unless the stars start close enough to the MBH, they will be scattered off their orbit. We identified a critical length scale a_c which demarcates the volume from which inspiral is possible. We obtained an analytical expression for the inspiral rate and showed that it is of the order of a few per Gyr per galaxy, much smaller than the rate for direct capture (Alexander & Hopman 2003), that it is nearly independent of the relaxation time for typical stellar cusps, and that it grows slowly with decreasing MBH mass (assuming the $M_\bullet - \sigma$ relation). Throughout we assumed a single powerlaw DF. Generalization to different profiles is straightforward. Qualitatively, the inspiral rate is determined by the stellar density near a_c , and is not very sensitive to the exact profile far away at radii much smaller or much larger than a_c . The rate of GW events depends on the number of COs inside a_c (which is much smaller than the MBH radius of influence), and so mass-segregation can play an important role in enhancing the event rate by leading to a centrally concentrated distribution of COs.

We obtained a relatively low rate. One important reason for this is our stringent criterion for inspiral. This may also explain why our results deviate from Hills & Bender 1995, although they do not specify their precise criterion for inspiral. Comparison with other works are more complicated. Possible differences may stem from different normalizations of the central density, different CO fractions, different criteria for inspiral, and the way mass segregation is treated. An essential step in the future will be to analyze inspiral processes by N-body simulations, which are feasible already for small systems (Baumgardt et al. 2004a, 2004b; Preto et al. 2004).

The detection rate depends on the inspiral rates, but also on the mass, relaxation time, the orbital parameters (especially the eccentricity) and the details of the detection algorithm (Barack & Cutler 2003). Here we provide a simple recipe to estimate the number of detectable sources. We assume that the various dependencies above can be expressed by an effective strain \hat{h} .

The strain of GW resulting from a star of mass $M_\star = m M_\odot$ orbiting a MBH of mass $M_\bullet = 10^6 M_\odot M_6 \gg M_\star$ at a distance $d = \text{Gpc } d_{\text{Gpc}}$, on a circular orbit of orbital frequency $\nu = 10^{-3} \text{s}^{-1} \nu_{-3}$, is given by

$$h = 1.7 \times 10^{-23} \nu_{-3}^{2/3} d_{\text{Gpc}}^{-1} M_6^{2/3} m. \quad (49)$$

The cosmic rate of *LISA* events is given by

$$\Gamma_{\text{tot}} = \int_{M_{\min}}^{M_{\max}} dM_\bullet \frac{dn_\bullet}{dM_\bullet} \Gamma_i(M_\bullet) V(M_\bullet), \quad (50)$$

where dn_\bullet/dM_\bullet is the number of MBHs per unit mass, per unit volume, and $V(M_\bullet)$ is the volume in which stars can be observed by *LISA*. Aller & Richstone (2002) used the $M_\bullet - \sigma$ relation to “weigh” the MBHs. The spectrum is roughly approximated by

$$\frac{dn_\bullet}{dM_\bullet} = 10^7 \left(\frac{1}{10^6 M_\odot} \right) M_6^{-1} \text{Gpc}^{-3}. \quad (51)$$

The *LISA* sensitivity curve at $\nu = 10^{-3}$ is $h \sim 10^{-23}$. We adopt this value as a representative detection threshold for \hat{h} . If the effective strain has to be at least $10^{-23} \hat{h}_{-23}$ for the star to be observable, then, for a Euclidean Universe,

$$V(M_\bullet) = 20.6 \text{Gpc}^3 \hat{h}_{-23}^{-3} \nu_{-3}^2 m^3 M_6^2. \quad (52)$$

Finally, the rate per MBH is

$$\Gamma_i(M_\bullet) = \Gamma_i(3 \times 10^6 M_\odot) (3M_6)^{-1/4}, \quad (53)$$

where we used the expression for the dependence of the inspiral rate on the MBH mass, equation (35), with $\beta = 4$. The expression can be calibrated with the MC results for a $3 \times 10^6 M_\odot$ MBH.

Integrating (50) from $M_6 = 0.5$ to $M_6 = 5$ gives

$$\Gamma_{\text{tot}} = 1.5 \text{yr}^{-1} \left[\frac{\Gamma_i(3 \times 10^6 M_\odot)}{\text{Gyr}^{-1}} \right] m^3 \hat{h}_{-23}^{-3} \nu_{-3}^2. \quad (54)$$

The number of sources which *LISA* can observe at any moment is estimated by $\mathcal{N} = \Gamma_{\text{tot}} \times t_L(\bar{e}, a_L)$, where t_L is the time a star with eccentricity \bar{e} spends in the *LISA* band before being swallowed; here \bar{e} is the average eccentricity of stars entering the *LISA* band.

For example, our calculations for WD inspiral indicate that $\Gamma_i(3 \times 10^6 M_\odot) = 7.8 \text{Gyr}^{-1}$. For a circular orbit with a period of $P = 10^3 \text{s}$ and $M_6 = 1$, the inspiral time is $t_L = 54 \text{yr}$, in which case the number of detectable sources would be $\mathcal{N} \sim 130 \hat{h}_{-23}^{-3} \nu_{-3}^2$.

We would like to emphasize that this estimate is to be treated with caution. The number of detectable sources depends strongly on the assumptions. In particular, GWs from eccentric sources are not monochromatic and may be harder to detect. The analysis in this paper can be used for a more detailed analysis of the number of detectable *LISA* sources.

We used three complementary methods to model the inspiral process, MC simulations, numerical solution of the diffusion/dissipation equation and an analytic effective orbit model. We followed the evolution of the orbital properties of the inspiraling stars to the point where they decoupled from the scattering. All three methods were in excellent agreement. We find that the distribution of orbital angular momenta is strongly peaked near $J \gtrsim J_{lc}$, with the detailed form of the distribution depending somewhat on the parameters of the stellar system. We demonstrated that estimates that “freeze” the scattering prematurely may lead to erroneously high rates by counting stars that actually plunge into the MBH. We then used the most versatile method, the MC simulations, to con-

tinue evolving the orbits in a GR Schwarzschild potential, taking into account energy and angular momentum loss due to GW emission (and residual perturbations by scattering). We derived the distribution of eccentricities of the inspiraling stars as they enter the detection window (orbital period of $P_L \lesssim 10^4$ s for *LISA*).

Our main result is that the eccentricities of stars entering the *LISA* band are strongly skewed toward high values.

TA is supported by ISF grant 295/02-1, Minerva grant 8484, and a New Faculty grant by Sir H. Djangoly, CBE, of London, UK.

REFERENCES

- Alexander, T., 1999, *ApJ*, 520, 137
 Alexander, T., & Morris, M., 2003, *ApJ*, 590, L25
 Alexander, T., & Hopman, C., 2003, *ApJ*, 590, L29
 Aller, M. C., & Richstone, D., 2002, *AJ*, 124, 3035
 Bahcall, J. N., & Wolf, R. A., 1976, *ApJ*, 209, 214
 Bahcall, J. N., & Wolf, R. A., 1977, *ApJ*, 216, 883
 Barack, L., & Cutler, C., 2004, *PRD*, 69, 082005
 Barack, L., & Cutler, C., 2004, *gr-qc/0409010*
 Baumgardt, H., Makino, J., & Ebisuzaki, T., 2004a, *ApJ*, 613, 1133
 Baumgardt, H., Makino, J., & Ebisuzaki, T., 2004b, *ApJ*, 613, 1143
 Binney, J. & Tremaine, S., 1987, *Galactic Dynamics* (Princeton: Princeton Univ. Press)
 Cohn, H., & Kulsrud, R. M. 1978, *ApJ*, 226, 1087
 Cutler, C., Kennefick, D., & Poisson, E., 1994, *PRD*, 50, 6
 Ferrarese, L., & Merritt, D., 2000, *ApJ*, 539, L9
 Figier, D. F., Kim, S. S., Morris, M., Serabyn, E., Rich, R. M., & McLean, I. S. 1999, *ApJ*, 525, 750
 Frank, J., & Rees, M. J., 1976, *MNRAS*, 176, 633
 Freitag, M., & Benz, W., 2001, *A&A*, 375, 711
 Freitag, M., 2001, *Class. Quantum Grav.*, 18, 4033
 Freitag, M., 2003, *ApJ*, 583, L21
 Freitag, M. & Benz, W., 2002, *A&A*, 394, 345
 Gair, J. R., Barack, L., Creighton, T., Cutler, C., Larson, S., L., Phinney, E. S., Vallisneri, M., 2004, *gr-qc/0405137*
 Gebhardt, K., et al., 2000, *ApJ*, 539, L13
 Gebhardt, K., et al. 2003, *ApJ*, 583, 92
 Genzel, R. et al., 2003, *ApJ*, 594, 812
 Genzel, R., Schödel, R., Ott, T., Eckart, A., Alexander, T., Lacombe, F., Rouan, D., & Aschenbach, B., 2003, *Nature*, 425, 934
 Glampedakis, K., Hughes, S. A., & Kennefick, D., 2002, *Phys. Rev. D*, 66, 064005
 Hills, D., & Bender, P. L., 1995, *ApJ*, 445, L7
 Hopman, C., Portegies Zwart, S.F., & Alexander, T., 2004, *ApJ*, 604, L101
 Ivanov, P. B., 2002, *MNRAS*, 336, 373, 2002
 Lightman, A. P., & Shapiro, S. L., 1977, *ApJ*, 211, 244
 Madau, P., & Rees, M. J., 2001, *ApJ*, 551, L27
 Magorrian, J., & Tremaine, S., 1999, *MNRAS*, 309, 447
 Miller, M. C., & Colbert, J. M., 2004, *Int.J.Mod.Phys. D* 13 1-64
 Miller, J. M., Fabian, A. C., & Miller, M. C., 2004, 614, *ApJ*, L117
 Miralda-Escudé, J., & Gould, A., 2000, *ApJ*, 545, 847
 Mouawad, N., Eckart, A., Pfalzner, S., Schödel, R., Moutaka, J., Spurzem, R., 2004, *Astronomische Nachrichten*, Vol. 326, 2, 83-95
 Peebles, P. J. E., 1972, *ApJ*, 178, 371
 Peters, P. C. 1964, *Phys. Rev.*, 136, 1224
 Piero, V., Pinto, I. M., Spallicci, A. D., Laserra, E., Recano, F., 2001, *MNRAS*, 325, 358
 Portegies Zwart, S. F., McMillan, S. L. W. 2002, *ApJ*, 576, 99
 Portegies Zwart, S. F., Baumgardt, H., Makino, J., McMillan, S. L., & Hut, P., *Nature*, 428, 724
 Press, W. H., Teukolsky, S. A., Vetterling, W. T., & Flannery, B. P. 1992, (Cambridge: University Press), 2nd ed.
 Press, W. H., & Teukolsky, S. A., *ApJ*, 213, 183
 Preto, M., Merritt, D., Spurzem, R., 2004, *ApJ*, 613, L109
 Quinlan, G. D., Hernquist, L., & Sigurdsson, S., 1995, *ApJ*, 440, 554
 Sigurdsson, S., *astro-ph/0304251*
 Sigurdsson, S., and Rees, M. J., 1997, *MNRAS* 284, 318
 Syer, D., & Ulmer, A., 1999, *MNRAS*, 306, 35
 Tremaine, S., et al., 2002, *ApJ*, 574, 740
 Wang, J., & Merritt, D., 2004, *ApJ*, 600, 149
 Wen & Gair, 2005, pre-print: *gr-qc/0502100*
 Young, P., 1980, *ApJ*, 242, 1232
 Zhao, H.-S., Haehnelt, M. G., & Rees, M. J., 2002, *New Astron.*, 7, 385